01 Sep 2009

On the Transition Rate of the Fe X RED Coronal Line

Gunter Brenner

Jose R. Crespo Lopez-Urrutia

Sven Bernitt

Daniel Fischer
Missouri University of Science and Technology, fischerda@mst.edu

et. al. For a complete list of authors, see https://scholarsmine.mst.edu/phys_facwork/766

Recommended Citation

G. Brenner and J. R. Crespo Lopez-Urrutia and S. Bernitt and D. Fischer and R. Ginzel and K. U. Kuhnel and V. Mackel and P. H. Mokler and M. C. Simon and J. H. Ullrich, "On the Transition Rate of the Fe X RED Coronal Line," *Astrophysical Journal*, vol. 703, no. 1, pp. 68-73, Institute of Physics - IOP Publishing, Sep 2009.
The definitive version is available at https://doi.org/10.1088/0004-637X/703/1/68

The Astrophysical Journal, 703:68–73, 2009 September 20 doi:10.1088/0004-637X/703/1/68

ON THE TRANSITION RATE OF THE Fe x RED CORONAL LINE

G. Brenner, J. R. Crespo López-Urrutia, S. Bernitt, D. Fischer, R. Ginzel, K. Kubiček, V. Mäckel, P. H. Mokler, M. C. Simon, and J. Ullrich
Max-Planck-Institut für Kernphysik, Saupfercheckweg 1, D-69117 Heidelberg, Germany; crespojr@mpi-hd.mpg.de
Received 2009 April 28; accepted 2009 July 23; published 2009 August 25

ABSTRACT

We present a lifetime measurement of the $3s^2 3p^5\ ^2P^o_{1/2}$ first excited fine-structure level of the ground state configuration in chlorine-like Fe x, which relaxes to the ground state through a magnetic dipole ($M1$) transition (the so-called red coronal line) with a wavelength accurately determined to 637.454(1) nm. Moreover, the Zeeman splitting of line was observed. The lifetime of 14.2(2) ms is the most precise one measured in the red wavelength region and agrees well with advanced theoretical predictions and an empirically scaled interpolation based on experimental values from the same isoelectronic sequence.

Key words: atomic data – atomic processes – line: profiles – plasmas – stars: coronae – Sun: corona

1. INTRODUCTION

In a paper submitted in the year 1942, Edlén (1943) explained conclusively the strongest lines observed in the corona during solar eclipses following a suggestion contained in a letter sent to him already in 1937 (Edlén 1945) by W. Grotrian, which also had made essential contributions (Grotrian 1939) to this subject. Electric dipole forbidden transitions between fine-structure levels of the ground state configuration in multiply charged heavy ions were the origin of those, until then ununderstood, spectral features. Since then, such lines have retained a central role in astrophysics. The most prominent are the so-called *green* and *red iron line* originating from the magnetic dipole ($M1$) transitions $3s^2 3p^2\ P^o_{1/2} - ^2P^o_{3/2}$ in aluminum-like iron (Fe XIV) and $3s^2 3p^5\ ^2P^o_{3/2} - ^2P^o_{1/2}$ in chlorine-like iron (Fe X) at wavelengths of 530.29 nm and 637.45 nm, respectively (Kaufman & Sugar 1986). These two lines are of great interest for plasma diagnostics as they cannot only be found in the solar corona but have also been observed, e.g., in Seyfert galaxies (Osterbrock 1981), symbiotic stars (Wallerstein & Brugel 1988), and supernova remnants (Woodgate et al. 1974). In order to enable quantitative modeling of astrophysical and laboratory plasmas, a precise knowledge of the transition rates as well as the energies of these two prominent lines is indispensable. For example, if the radiative transition rate and collision strength are known, the intensity of the transition line may serve as a local temperature diagnostics of the plasma (Lynch & Kafatos 1991). Apart from the great relevance in plasma diagnostics and astrophysics, the studies of lifetimes of atomic states in multiply charged ions are of fundamental interest since new high precision lifetime measurements provide complementary information on the atomic structure as they are sensitive on the complete spatial distribution of the electronic wave functions and can therefore probe atomic structure calculations.

Recently, the lifetime of the $1s^2 2s^2 2p\ ^2P^o_{3/2}$ metastable level in boron-like Ar XIV (Lapierre et al. 2005, 2006) and the above mentioned $3s^2 3p\ ^2P^o_{3/2}$ level in Fe XIV (Brenner et al. 2007)—both decaying via a $M1$ transition—were measured by means of an electron beam ion trap (EBIT) resulting in an accuracy in the order of 0.1%, and thus becoming for the first time even sensitive on the quantum electrodynamic (QED) effect of the electron anomalous magnetic moment (EAMM), which contributes to 0.45% to the lifetime of these metastable states (Tupitsyn et al. 2005). In order to achieve this accuracy, many different tests of the ion loss rate were performed to rule out any systematic effects compromising the final results. The outstandingly accurate results of $9.573(4)(^{+12}_{-5})$ ms (stat)(syst) for Ar XIV and $16.726(^{+20}_{-10})$ ms for Fe XIV showed an unexplained small discrepancy on the order of 0.3% to the average value of existing calculations which in both cases predict a shorter lifetime.

Regarding the lifetime of the metastable state of the Fe x red coronal line discussed in this paper, two experiment-based values have been so far reported. One direct measurement was performed with an electrostatic Kingdon trap by Moehs et al. (Moehs & Church 1999) yielded a lifetime of 13.64(25) ms in strong disagreement with the trend of predictions, which in most cases had been adjusted for the experimental transition energy and in general infer a longer lifetime (Träbert 2004). Another lifetime value (Träbert 2004) which resulted from an extrapolation of values obtained in a study along the Cl I isoelectronic sequence (Co XI, Ni XII, and Cu XIII), later published in Träbert et al. (2006), was measured utilizing the heavy-ion storage ring technique at the Heidelberg Test Storage Ring (TSR). The extrapolated value for Fe x of 14.40(14) ms matches within error bars most calculations which are empirically adjusted to the measured wavelengths. However, this result is definitively at variance with the Kingdon trap result (Moehs & Church 1999). As no further direct measurement of the transition rate of the red coronal line (particularly also no measurement with an EBIT) was so far reported, and in view of the serious disagreement of the only available direct experimental value with theory, the aim of this work was to provide a crucial experimental data point as a guidance for further theoretical investigations on transition rates of forbidden lines in multielectron systems. Independently, the transition energy of the Fe red coronal line was determined with five times higher precision than existing data using the same technique as earlier EBIT work (Draganić et al. 2003; Soria Orts et al. 2006, 2007).

2. LIFETIME MEASUREMENT PROCEDURE

The measurement was carried out at the EBIT (HD-EBIT) located at the Max-Planck-Institut für Kernphysik in Heidelberg. The experiment follows the principle introduced by Wargelin and coworkers (Wargelin et al. 1993) at the LLNL EBIT, which initially was applied to X-ray forbidden transitions (Stefanelli

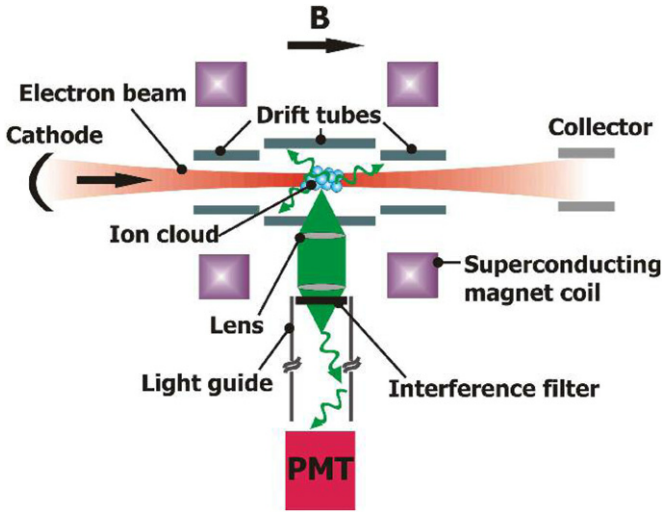

Figure 1. Illustration of the experimental set up at the EBIT; for explanation see the text. (The electron beam from the thermoionic cathode is switched off and on by an adjacent electrode not shown in the picture.)

et al. 1995; Beiersdorfer et al. 1996; Crespo López-Urrutia et al. 1998), and soon after at NIST (Serpa et al. 1997, 1998) and LLNL (Träbert et al. 2000) also to visible forbidden transitions. Our setup at the Heidelberg EBIT has already been described in earlier publications in great detail (Lapierre et al. 2005, 2006; Brenner et al. 2007), and only the essentials of the lifetime measurement procedure (shown in Figure 1) will be sketched in the following.

Basically, Fe x ions are produced through electron impact ionization by an electron beam originating from the cathode of an electron gun. A 8 T magnetic field produced by a pair of superconducting Helmholtz coils highly compresses the electron beam at the trap center to a diameter of roughly 50 μm. The negative space charge potential of the electron beam traps the ions in the radial direction while the axial confinement is achieved by means of a set of cylindrical electrodes (drift tubes) biased to an appropriate potential. The electron beam successively brings Fe atoms, which are injected into the trap region as a molecular beam of iron pentacarbonyl, $Fe(CO)_5$, to the desired charge state. As the ionization potential of Fe IX is 232.5 eV, the effective electron beam energy at the trap center was set to 242 eV, well below the ionization potential of the next higher charge state (262.1 eV) but sufficient to produce Fe x. Due to this low energy of the electron beam the electron emission current was set to a maximum of 13 mA to ensure stable electron beam conditions. Furthermore, to avoid charge exchange processes due to residual gas atoms in the trap, throughout the measurement the pressure of the highly collimated, fivefold differentially pumped gas injection system was kept constantly on a low level of 5×10^{-8} torr already in the first pumping stage. After passing two stages pumped by turbomolecular pumps, and three more cryogenically pumped at 50 K, 20 K, and 4.2 K, the molecular beam density at the trap is estimated at 10^7 cm^{-3}. The density of residual gas due to other sources at the trap lies well below 10^6 cm^{-3}.

In order to efficiently detect the fluorescence light emitted by the ions upon deexcitation, a lens system installed inside of the EBIT vacuum chamber collects the fluorescence photons and produces an intermediate image of the ion ensemble outside of the window. The light is then guided through an $\cong$1 m long aluminum tube with a highly polished inner reflecting surface to a Peltier cooled photomultiplier tube (PMT) with a dark count rate of 30 s^{-1}. To select the Fe x spectral line, a narrow band interference filter with 10 nm full width at half-maximum (FWHM) having a transmission of 60% at a center wavelength of 640 nm is installed in front of the PMT. Furthermore, the interference filter prevents stray light of other wavelengths from reaching the detector. As the glow of the thermionic cathode ($T \approx 1300$ K) produces some stray light matching the transmission range of the interference filter, the cathode filament voltage was reduced to the minimum value needed to attain the desired emission current. However, even by driving the cathode filament at the lowest voltage possible, the background count rate of the PMT increased to about 200 s^{-1}. Therefore, the cathode temperature is the main source of background, with interesting consequences which will be discussed below. This high background limits the achievable accuracy of the measured lifetime.

Similar to previous EBIT lifetime measurements on Ar XIV and Fe XIV, the lifetime of the metastable $3s^2 3p^5\ ^2P^o_{1/2}$ energy level was deduced from the analysis of optical fluorescence decay curves following from deexcitation to the $3s^2 3p^5\ ^2P^o_{3/2}$ ground state via a magnetic dipole ($M1$) transition with a transition wavelength of $\lambda = 637.451$ nm (air) (Shirai et al. 2000), the aforementioned *red coronal line* from Fe x. The decay curves are obtained by cyclically turning the electron beam on for 1100 ms and off for 400 ms, therefore operating the EBIT in the so-called magnetic trapping mode (Beiersdorfer et al. 1996) during the electron beam-off phase. In order to suppress axial ion losses during the off phase, an electrostatic potential of 1000 V was applied to the two drift tubes closest to the trap center, which was sufficient to keep the ions in the trap axially confined while the electron beam is off (Brenner et al. 2007). Because of the relatively high background signal level on the PMT due to the glow of the cathode, and also in view of the moderately small expected fluorescence count rate, it was indispensable to improve the signal-to-noise ratio as far as possible. This was achieved by changing the trap depth cyclically, for details see Brenner et al. (2007). While the electron beam is on (ionization and excitation period), the two innermost drift tubes were set to 0 V potential (shallow trap configuration), leading to a cooler ion ensemble and an enhanced ionization rate, thus increasing the overall signal rate. Just 200 ms before switching off the electron beam, the trapping potentials of the two drift tubes were raised to 1000 V. This deep trap configuration was kept until 300 ms after the electron beam was turned on again. The decrease of the measured photon flux with time after the electron beam is switched off reflects basically only the decay of the metastable Fe x ions.

3. WAVELENGTH AND ION TEMPERATURE DETERMINATION

The line originating from the $M1$ transition $3s^2 3p^5\ ^2P^o_{3/2} - 3s^2 3p^5\ ^2P^o_{1/2}$ splits in the presence of a magnetic field, as the fine-structure energy levels $^2P^o_{3/2}$ and $^2P^o_{1/2}$ are split into magnetic sublevels; the transition exhibits six Zeeman components. Until recently, Zeeman splitting had been observed for highly charged heavy ions only in the case of Ar XIV, both in a tokamak (Iwamae et al. 2007) and in an EBIT (Soria Orts et al. 2006, 2007).

In order to verify that Fe x is produced in the ion trap and to check whether further spectral lines originating from any other ion species present in the trap having a wavelength similar to the line of interest, a wavelength measurement

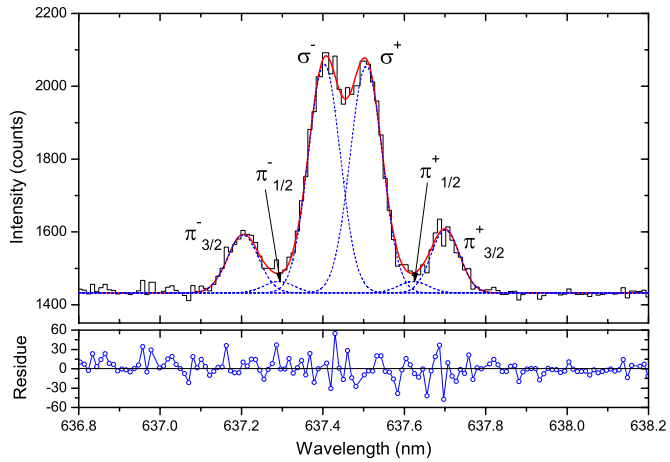

Figure 2. Recording of the $M1\ 3s^2 3p^2\ P^o_{3/2} - 3s^2 3p^2\ P^o_{1/2}$ spectral line in Cl-like Fe x showing its Zeeman components in the 8 T magnetic field of the EBIT.

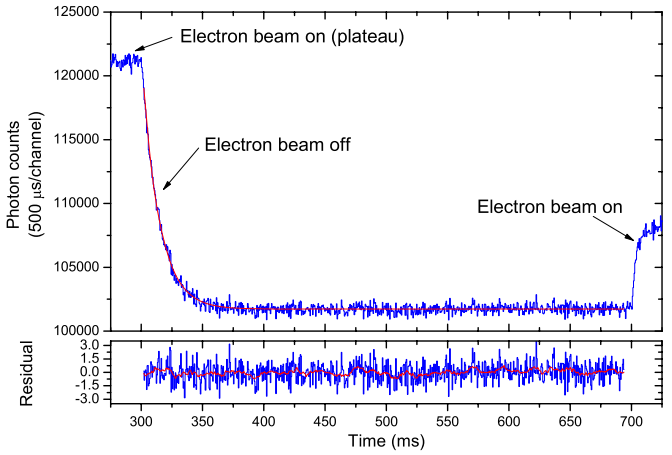

Figure 3. Lifetime fluorescence decay curve of the $3s^2 3p^2\ P^o_{3/2}$ level (10-fold binning) and residual from single exponential fit (bottom). The electron beam was turned off for 400 ms at a measurement cycle of 1500 ms. The total data acquisition time was 83 hr.

of the lines was carried out with an optical Czerny–Turner spectrometer equipped with a 1800 l mm^{-1} grating and a cryogenically cooled charged coupled device (CCD) camera (2000 × 800 pixel). From the recorded spectra, the transition wavelength was determined, and the presence of Fe x confirmed. Detailed descriptions of the wavelength measurement setup are found in Draganić et al. (2003) and Soria Orts et al. (2006, 2007). Furthermore, this setup was also used to optimize the trapping parameters and the settings for the lifetime measurement.

The spectrometer calibration was performed by means of an iron hollow cathode lamp filled with neon carrier gas. The positions of eight Ne I lines from the calibration spectra covering the region of interest were determined by fitting Gaussian functions and plotted against their well known wavelengths taken from the NIST database (Ralchenko et al. 2008). The instrumental dispersion curve was obtained by fitting a second-order polynomial to the data. A typical spectrum is shown in Figure 2. Apart from the expected spectral line of the $^2P^o_{1/2} - ^2P^o_{3/2}$ transition in Fe x, no other lines could be found in the spectrum within the bandwidth of the interference filter that was used in the lifetime measurement. The exposure time for the spectrum shown was 60 minutes and the electron emission current was chosen to be 13 mA low (beam constantly on) in order to reduce heating of the ions. Moreover, for this measurement the two innermost drift tubes were set to a moderately low potential of 100 V in order to enhance evaporative cooling and keep the ion temperature low, thus reducing the Doppler broadening. In this way, it was possible to resolve the individual Zeeman components. The spectrum shows the expected Zeeman pattern. While the $\pi_{3/2}$-components and the σ-components are clearly revealed, the $\pi_{1/2}$-components could not be completely resolved due to the instrumental width of the recorded lines, which was basically the consequence of the entrance slit width of the spectrometer and of the ion temperature. However, the six components could be fitted by Gaussians, assuming that the FWHM of these six Zeeman components are equal. To determine the center of gravity of the spectral line, either the outer $\pi_{3/2}$-components or the inner σ-components can be used, thus resulting in two wavelength values. The wavelength of the red coronal line is obtained by the statistically weighted average of the above deduced two wavelength values. The result of 637.454(1) nm is in perfect agreement with, but five times more accurate than the experimentally obtained value of 637.457(5) nm reported by Del Zanna et al., who reviewed and assessed available atomic data on Fe x for astrophysical applications (Zanna et al. 2004).

The Doppler broadening of the individual Zeeman components directly reflects the ion temperature in the trap. Assuming a Maxwellian distribution, the ion temperature T_i and a Doppler broadening of the spectral line with a Gaussian width W_D are connected by the following relation:

$$T_i = \frac{M_i c^2}{8 k_B \ln 2} \left(\frac{W_D}{\lambda_0} \right)^2 , \quad (1)$$

where λ_0 is the central wavelength, k_B is the Boltzmann constant, M_i is the atomic mass of the ion, and c is the speed of light. The line width W_0 observed in the spectra therefore not only results from the natural line width W_i but mainly from the Doppler broadening W_D and the finite instrumental resolution W_r. As for this forbidden transition, the natural line width W_i is negligibly small, the line shape is mainly determined by the two largest effects, W_D and W_r, both of which can be described by Gaussians. Hence, to obtain the Doppler broadening W_D these contributions were deconvoluted by means of the following expression: $W_D = \sqrt{W_0^2 - W_r^2}$. The instrumental response profile W_r was carried out from the calibration spectra and lead to a value of 0.031(1) nm. Deducing the total width W_0 from the four resolved Zeeman components to be in average 0.076(7) nm, the observed Doppler width W_D results in 0.069(8) nm. Therefore, according to Equation (1) the temperature of the trapped ions was $T_i = 110(25)$ eV, which is a reasonable value for the axial trap potential applied.

4. LIFETIME DETERMINATION

A typical lifetime decay curve is shown in Figure 3. The total acquisition time for this curve was 83 hr. During this time all settings, like, e.g., the electron beam energy (242 eV), electron beam current (13 mA), and first stage gas injection pressure (4.9×10^{-8} torr), were kept stable. The trapping potential was simultaneously switched with the electron beam between 0 V and 1000 V according to the above given time periods. The red curve in the graph represents a first-order exponential

fit function

$$N(t) = a_1 \exp(-t/t_1) + b_1 t + y_0 \quad (2)$$

with free parameters a_1, t_1, and y_0 representing the initial intensity, the decay time, and the measured PMT background rate, respectively. The additional term $b_1 t$ accounts for an additional slightly positive slope of $b_1 = (0.35 \pm 0.13)\ \mathrm{s}^{-1}$ of the background level which will be discussed below in further detail.

The obtained χ^2/degrees of freedom (DOF) and R^2 of the fit were 1.08 and 0.977. Fitting the data with any other higher order exponential function including two or more exponentials did not yield convergent results, thus indicating that no other decay component is superimposed with the decay curve originating from the $M1$ line of Fe x. To avoid any systemic effects due to instabilities during switching of the electron beam, the fitting procedure was always started 2 ms after the electron beam was switched off. The data were subjected to a standard tail-fit analysis by truncating the starting point of the fit from 2 ms up to 28 ms after turning off the electron beam. This test showed only fluctuations consistent with the statistical uncertainties.

The dead time of the data acquisition system including PMT, preamplifier, and discriminator was measured to be $t_d = 1.5(1)\ \mu$s. The dead time effect was corrected using the relation $N_c(t) = N(t)/(1 + N(t)t_d/t_a)$, where N_c is the number of photons counted by the data acquisition system and t_a is the total acquisition time per channel.

Taking into account the statistical uncertainty only, the deduced lifetime from this measurement is 14.19(17) ms, with a relative accuracy of 1.2%.

5. SYSTEMATIC EFFECTS ON THE LIFETIME

The measured lifetime can be affected by various systematic effects, like, e.g., ion losses from the trap, charge exchange recombination, repopulation of the level of interest by cascades, change in the background photon flux, etc. Extended studies on possible systematic error sources in lifetime measurements at the HD-EBIT have already been carried out on the above mentioned levels of 0.1% in Ar XIV and Fe XIV, and have been described in great detail in earlier publications (Lapierre et al. 2005, 2006; Brenner et al. 2007).

The axial ion loss from the trap can be discarded as the applied electrostatic potential of 1000 V on the two innermost drift tubes is large enough to keep the ion loss rate many orders of magnitude smaller than the measured transition rate (Lapierre et al. 2005, 2006; Brenner et al. 2007). Furthermore, radial ion losses can also be excluded as the effect of transverse cross-field diffusion in the given strong magnetic field is too small to affect the measurement (Lapierre et al. 2006). For clarity, we like to add here that while switching to the magnetic trapping mode the ion cloud expands to slightly larger radii and after switching on the electron beam again not the complete ion cloud is overlapped with it. This leads to the lower photon flux level seen at the end of the measuring period shown in Figure 3. As demonstrated earlier (Lapierre et al. 2006; Brenner et al. 2007) this is not connected with any ion loss during the measuring period, since the expanding ion cloud containing the metastables completely remains within the field of view of the fluorescence detection system.

The ionic charge state can change due to charge exchange of the ions with neutral atoms of the residual gas. This would lead to a loss of Fe x ions, and consequently, to an apparent lifetime shorter than the natural one. Conversely, electron capture by higher ionized Fe ions would generate Fe x ions. This is prevented by choosing an electron beam energy below the ionization potential of Fe x, so no higher charge state than Fe x was present in the trap. The influence of the charge exchange effect on the measured lifetime was experimentally checked during the lifetime determination of metastable states in Ar XIV and Fe XIV at the EBIT by recording several decay curves at different gas injection pressures, and thus at different number densities in the trapping region (Lapierre et al. 2005, 2006; Brenner et al. 2007). At the 0.1% accuracy level, no shifts due to charge exchange were detected there. Thus, we are confident that also in the present case charge exchange does not affect the measured lifetime.

Cascade repopulation of the $3p^5\ ^2P^o_{1/2}$ metastable level by transition from higher lying levels having a lifetime similar to the level of interest could in principle influence the measured decay curve. However, the analysis of the Fe x spectrum show that there are only seven levels within the $3s^2\ 3p^4\ 3d$ configuration with lifetimes in the millisecond range ($^4D_{7/2}$, $^4F_{9/2}$, $^4F_{7/2}$, $(3P)^2F_{7/2}$, $^2G_{9/2}$, $^2G_{7/2}$, $(1D)^2F_{7/2}$) (Huang et al. 1983). All these various long-living $3d$ levels decaying via $M1$, $E2$, and $M2$ transitions feature transition energies ranging from the EUV into the visible spectral region (30–350 nm) and therefore, cannot directly contribute to the red coronal line within the bandwidth of the used interference filter at 640 nm. Inspecting the 98 transitions classified at the NIST database (Ralchenko et al. 2008) we did not find any relevant slow cascade channels populating the $3p^5\ ^2P^o_{1/2}$ metastable level. Anyhow, the corresponding excitation cross sections are small and hence the population of $3d$ levels is negligible compared with that of the ground state. Moreover, the measured decay curves do not show any structure which could be fitted by a multi-exponential function, indicating that none of the $3d$ levels contribute significantly to the lifetime of the upper ground state in Fe x.

In the light curves of these measurements a large photon background is present even within the wavelength region filtered, cf. Figure 2. The intensity due to the Fe x emission raises at the beginning only about 20% over the background level before decaying back to that level. Checking the background closely, one finds a small growth of the baseline, which was modeled using coefficient b_1 in Equation (2). In a heated thermionic cathode, the energy required to overcome the work function is provided by the thermal motion of the electrons in the bulk. Each electron acquiring through collisions enough kinetic energy to surpass the vacuum barrier thus removes energy from the cathode. When the electron beam is switched off, the electrons cannot carry energy away from the cathode, and the cathode will be heated up accordingly. If no current is extracted from the cathode, equilibrium between evaporating and recombining electrons ensures that no energy flow takes place. However, when a current is sustained, a net cooling effect results. This evaporative cooling had been early used to determine work functions (Heinze 1933) by measuring the cathode temperature through the changes in the heater filament resistance.

To investigate this minute, yet detectable contribution to the background of the photomultiplier signal, a detailed study of the cathode glow as a function of time was necessary. The cathode was modeled as a system of five discrete, thermally linked masses, representing the tungsten–barium dispenser cathode itself, the heating element mainly made of aluminum oxide, and different parts of the mounting, with one of them connected to a reservoir of constant temperature. Thermal

Table 1
Lifetimes and Decay Rates for the Red Coronal Line in Fe x, Top: Theoretical Values and Bottom: Experimental Results

τ (ms)	A (s^{-1})	Theoretical Method	Label on Figure 4	Reference
14.41	69.4	Scaled TF	1	Warner (1968)
14.41	69.4	HF	2	Smith & Wiese (1973)
14.46	69.15	HF	3	Czyzak et al. (1974)
14.41	69.4	CA	4	Kastner (1976)
14.46	69.15	CD	5	Kafatos & Lynch (1980)
14.37	69.59	CD	6	Eidelsberg et al. (1981)
14.44	69.25	MCDF	7	Huang et al. (1983)
14.41	69.4	SS	8	Kaufman & Sugar (1986)
18.21	54.91	SS	9	Bhatia & Doschek (1995)
15.29	65.4	MCDF	10	Dong et al. (1999)
14.54	68.78	CI	11	Moehs et al. (2001)
		Semiempirical Method		
14.41(0.14)	69.4(0.67)	Extrapolation TSR	13	Träbert et al. (2002)
		Experimental Method		
13.64(0.25)	73.31(1.32)	Kingdon	12	Moehs & Church (1999)
14.2(0.2)	70.4(1.0)	HD-EBIT	14	This work

Notes. Column 4: labels on data points in Figure 4. Theoretical models used: HF, Hartree–Fock; TF, Thomas–Fermi; CA, Coulomb approximation; CD, compiled data; MCDF, multi configuration Dirac–Fock; SS, SUPERSTRUCTURE; CI, configuration interaction.

radiation was considered, according to the Stefan–Boltzmann law. The energy deposition by the filament heater and the energy loss due to emitted electrons were both included. The resulting set of differential equations was solved using a Runge–Kutta numerical integrator. In the simulation, first a realistic equilibrium temperature of about 1300 K was obtained. Then, switching on and off the electron emission periodically a temperature increase of 0.16 K is predicted for the beam-off period leading to an increase of the photon flux by about 0.20% for the red visible light region at 637(10) nm. The rise in intensity is approximately linear in the short 400 ms beam-off period, and perfectly explains our observations, and in particular the value of the coefficient b_1 deduced from the linear background increase observed in the decay curve. This effect will be used in future investigations to determine directly the work function of the heated cathode.

6. SUMMARY

The wavelength region of the red coronal line of Fe x at 637.454(1) nm is a difficult one: at this region not only the low quantum efficiency of the PMT is disadvantageous, but even more so the intensive photon background emitted by the hot cathode of the electron gun. This background is also present during the measuring period with the electron beam in the trap itself being switched off, and causes a signal-to-background ratio nearly 2 orders of magnitude worse than in our earlier work. For this only reason, the final accuracy of the present EBIT measurement does not reach the level attained there (Lapierre et al. 2005, 2006; Brenner et al. 2007).

After understanding and modeling the background of the decay curve in great detail, the lifetime of the first excited level in Fe x was deduced with high accuracy to 14.2(2) ms, see Table 1. This value agrees within error bars with an extrapolation based on neighboring ion species measured at TSR (Träbert 2004). Results from a Kingdon trap yielding a shorter lifetime (Moehs & Church 1999), in contradiction with our more accurate results and with Träbert's extrapolation (Träbert 2004), may be explained by some loss mechanisms not taken into account in that experiment.

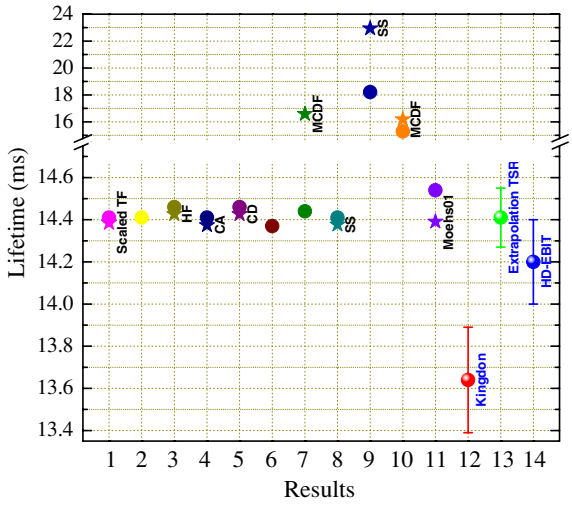

Figure 4. Comparison between predictions of the lifetime of the Fe x and experimental data from this and other groups. Theoretical values are presented as published (dots) and after applying corrections due to the experimental transition energy and the contribution of the anomalous electron magnetic moment (stars).

Due to the high background level, the accuracy of our measurement is not high enough to study the EAMM contribution to the transition probability. However, the experimental accuracy is sufficient to compare with available standard theories (see the top part of Table 1 and also Figure 4). Within error bars, our value and the TSR extrapolation agree well with most of the available theoretical results. Only two of them, the multi-configuration Dirac–Fock prediction (MCDF, number 10; Dong et al. 1999), and the one in Reference Bhatia & Doschek (1995) (SS, number 9) using the SUPERSTRUCTURE code originally developed by Eissner and coworkers (Eissner et al. 1974) deliver deviating results, asking for improvements in those calculations.

In summary, we have benchmarked the transition wavelength with an accuracy five times higher than earlier works to 637.454(1) nm for the $3s^2 3p^5\ ^2P^o_{1/2}$ first excited fine-structure level in chlorine-like Fe x, thus enhancing its applicability to velocity determinations based on Doppler shifts. Most importantly, the transition rate from this first excited state to the ground

state level in Fe x could be determined with high accuracy to 70.4(1.0) s^{-1}. This improved value solves the contradiction between extrapolated values along the same isoelectronic sequence and Kingdon trap measurements, confirms the validity of most predictions at a level sufficient for plasma density determinations, and discards the results of some of them, pointing to possible further inaccuracies of the methods underlying those disagreeing predictions in other cases where they have been applied.

REFERENCES

Beiersdorfer, P., Schweikhard, L., Crespo López-Urrutia, J. R., & Widmann, K. 1996, Rev. Sci. Instrum., 67, 3818
Bhatia, A. K., & Doschek, G. A. 1995, At. Data Nucl. Data Tables, 60, 97
Brenner, G., Crespo López-Urrutia, J. R., Harman, Z., Mokler, P. H., & Ullrich, J. 2007, Phys. Rev. A, 75, 032504
Crespo López-Urrutia, J. R., Beiersdorfer, P., Savin, D. W., & Widmann, K. 1998, Phys. Rev. A, 58, 238
Czyzak, S. J., Aller, L. H., & Euwema, R. N. 1974, ApJS, 28, 465
Dong, C. Z., Fritzsche, S., Fricke, B., & Sepp, W.-D. 1999, Mon. Not. R. Astron. Soc., 307, 809
Draganić, I., et al. 2003, Phys. Rev. Lett., 91, 183001
Edlén, B. 1943, Z. Astrophys., 22, 30
Edlén, B. 1945, Mon. Not. R. Astron. Soc., 105, 323
Eidelsberg, M., Crifo-Magnat, F., & Zeippen, C. J. 1981, A&A, 43, 455
Eissner, W., Jones, M., & Nussbaumer, H. 1974, Comput. Phys. Commun., 8, 270
Grotrian, W. 1939, Naturwissenschaften, 27, 214
Heinze, W. 1933, Ann. Phys., 408, 41
Huang, K.-N., Kim, Y.-K., Cheng, K., & Desclaux, J. P. 1983, At. Data Nucl. Data Tables, 28, 355
Iwamae, A., Atake, M., Sakaue, A., Katai, R., Goto, M., & Morita, S. 2007, Phys. Plasmas, 14, 042504
Kafatos, M., & Lynch, J. P. 1980, ApJ, 42, 611
Kastner, S. O. 1976, Sol. Phys., 46, 179
Kaufman, V., & Sugar, J. 1986, J. Phys. Chem. Ref. Data, 15, 321
Lapierre, A., et al. 2005, Phys. Rev. Lett., 95, 183001
Lapierre, A., et al. 2006, Phys. Rev. A, 73, 052507
Lynch, J. P., & Kafatos, M. 1991, ApJS, 76, 1169
Moehs, D. P., Bhatti, M. I., & Church, D. A. 2001, Phys. Rev. A, 63, 032515
Moehs, D. P., & Church, D. A. 1999, ApJ, 516, L111
Osterbrock, D. E. 1981, ApJ, 246, 696
Ralchenko, Y., et al. 2008, NIST Atomic Spectra Database version 3.1.5 (Gaithersburg, MD: NIST), http://physics.nist.gov/asd3
Serpa, F. G., Gillaspy, J. D., & Träbert, E. 1998, J. Phys. B, 31, 3345
Serpa, F. G., Morgan, C. A., Meyer, E. S., Gillaspy, J. D., Träbert, E., Church, D. A., & Takács, E. 1997, Phys. Rev. A, 55, 4196
Shirai, T., Sugar, J., Musgrove, A., & Wiese, W. L. 2000, J. Phys. Chem. Ref. Data, 8, 632
Smith, M. W., & Wiese, W. L. 1973, J. Phys. Chem. Ref. Data, 2, 85
Soria Orts, R., et al. 2006, Phys. Rev. Lett., 97, 103002
Soria Orts, R., et al. 2007, Phys. Rev. A, 76, 052501
Stefanelli, G. S., Beiersdorfer, P., Decaux, V., & Widmann, K. 1995, Phys. Rev. A, 52, 3651
Träbert, E. 2004, A&A, 415, L39
Träbert, E., Gwinner, G., Wolf, A., Knystautas, E. J., Garnir, H.-P., & Tordoir, X. 2002, J. Phys. B, 35, 671
Träbert, E., Reinhardt, S., Hoffmann, J., & Wolf, A. 2006, J. Phys. B: At. Mol. Phys., 39, 945
Träbert, E., et al. 2000, ApJ, 541, 506
Tupitsyn, I. I., Volotka, A. V., Glazov, D. A., Shabaev, V. M., Plunien, G., Crespo López-Urrutia, J., Lapierre, A., & Ullrich, J. 2005, Phys. Rev. A, 72, 062503
Wallerstein, G., & Brugel, E. W. 1988, A&A, 197, 182
Wargelin, B. J., Beiersdorfer, P., & Kahn, S. M. 1993, Phys. Rev. Lett., 71, 2196
Warner, B. 1968, Z. Astrophys., 69, 399
Woodgate, B. E., Stockman, H., Angel, J. R. P., & Kirshner, R. P. 1974, ApJ, 188, L79
Zanna, G. D., Berrington, K. A., & Mason, H. E. 2004, A&A, 422, 731